Journal of Materials Chemistry B

PAPER

View Article Online
View Journal | View Issue

Cite this: J. Mater. Chem. B, 2014, 2, 325

Layer-by-layer assembled graphene oxide composite films for enhanced mechanical properties and fibroblast cell affinity

Wei Qi,* Zhongyuan Xue, Wenjing Yuan and Hua Wang*

The mechanical properties of films are of great importance for their use as biocompatible surface coatings or for drug encapsulation and release. In this study, layer-by-layer (LbL) assembled graphene oxide (GO) nanocomposite films were constructed, aimed at improving the mechanical properties of polyelectrolyte multilayer (PEM) films containing poly(sodium 4-styrenesulfonate) (PSS) and poly(allylamine hydrochloride) (PAH). The mechanical properties of the films were evaluated *via* a nanoindentation technique. It was demonstrated that the elastic modulus (E_r) could be improved by up to 181% by one layer of GO deposition in ten bilayers of polyelectrolyte, while the E_r value of $[(PAH/GO)_{10}/PAH/PSS]_{30}$ film showed more than 5-fold enhancement over the native PEM film $(PAH/PSS)_{330}$. The hardness (H) also increased significantly, from 0.295 GPa to 2.79 GPa for the $(PAH/PSS)_{330}$ film and the $[(PAH/GO)_{10}/PAH/PSS]_{30}$ film, respectively. These results support the idea that the mechanical properties of the film could be tuned by varying the number of layers of GO in the multilayer architecture. Furthermore, the effect of the LbL-assembled GO composite films on fibroblast cell behavior was investigated. Cell proliferation and cell adhesion were qualified by MTT assay and fluorescent labeling using an image analysis system. Obviously, when compared with the native PEM films, the cells showed faster proliferation and larger spreading area, and formed more numerous and better organized adhesion points on the GO composite films. This indicated a higher affinity of fibroblasts for the LbL-assembled GO nanocomposites. The strategy promises a new way to construct nanofilms that are simultaneously mechanically rigid and bioactive, which is crucial for cell-contacting biomedical and biotechnological applications.

Received 7th October 2013
Accepted 30th October 2013

DOI: 10.1039/c3tb21387k

www.rsc.org/MaterialsB

1 Introduction

The layer-by-layer (LbL) adsorption technique, introduced 20 years ago, offers an easy and inexpensive process for multilayer formation and allows a variety of materials to be incorporated within the film structures.[1–3] The technique has led to a number of novel designs and applications, *e.g.*, chemical sensors, semipermeable membranes, drug delivery systems, superhydrophobic coatings and biomaterial coatings based on the fact that the nanostructure and properties of the LbL assemblies can be finely controlled.[4–9] For example, mechanical properties of the LbL-assembled films have been found to be dependent on the components of the films and on the assembly conditions of the films.[10–13]

In recent years, increasing efforts have been devoted to study the mechanical properties of films that they play key roles in a wide number of applications ranging from the coating of biomaterials and drug delivery capsules to understanding the mechanics of cell adhesion.[14–18] The investigation of mechanical properties is also of fundamental interest for providing insight into intermolecular interactions in the films.

In this study, an approach for the improvement of the mechanical properties of LbL polyelectrolyte multilayer (PEM) films has been introduced by incorporating graphene oxide (GO) into the polymeric matrix. GO has been employed widely in the fabrication of nanocomposite materials due to the easy functionalization of its structure.[19–21] The structure of GO is often simplistically assumed to be a graphene sheet bonded to oxygen in the form of carboxyl, hydroxyl, and epoxy groups. Graphene is an atom-thick sheet of carbon atoms arranged in a two-dimension honeycomb structure with fascinating electrical, thermal and mechanical properties.[22] For instance, an individual graphene nanosheet has been determined to exhibit extremely high values of Young's modulus (~1000 GPa), fracture strength (~125 GPa) and elastic modulus (~0.25 TPa).[23,24] Meanwhile, GO has received increasing interest for various applications including a variety of biomedical applications, such as cellular imaging, drug delivery, bioanalysis, stem cell

Key Laboratory of Life-Organic Analysis, Key Laboratory of Pharmaceutical Intermediates and Analysis of Natural Medicine, School of Chemistry and Chemical Engineering, Qufu Normal University, 57 Jingxuan West Road, Qufu, Shandong 273165, China. E-mail: qf_qw@163.com; huawangqfnu@126.com; Tel: +86 537 4458208; +86 537 4456306

research and photothermal therapy for tumors.[25–28] More recently, several researchers have investigated the self-assembly of two-dimensional GO into a three-dimensional macrostructure.[29–33]

Here, we fabricated nanocomposite films containing GO and poly(allylamine hydrochloride) (PAH) by LbL assembly to improve the mechanical properties of PEM films. The exfoliated GO nanosheets were used as building blocks, and the number of layers of GO was varied to tune the mechanical properties of the composite films. The loading of GO and film deposition was monitored using ultraviolet visible (UV-vis) spectroscopy and quartz crystal microbalance (QCM) techniques. The film homogeneity was characterized with atomic force microscopy (AFM) and the mechanical properties of the as-developed nanocomposite were evaluated by a nanoindentation method. It is known that alterations to the properties of films can promote cellular responses and affect cell–surface interactions along with cell growth and viability.[34] Accordingly, cell adhesion, cell viability and cell proliferation on the GO nanocomposites were investigated quantitatively and systematically by using fibroblast NIH-3T3 as a model. The major purpose of the work is to tune the mechanical properties of films by incorporating GO and further to investigate the effects of the nanocomposites on the cell behavior, as shown in Scheme 1.

2 Experimental

2.1 Materials

Polyethyleneimine (PEI, M_w: 25 000), poly(sodium 4-styrenesulfonate) (PSS, M_w: 70 000), and poly(allylamine hydrochloride) (PAH, M_w: 58 000) were purchased from Sigma-Aldrich (USA). Expandable graphite (EG) 8099200 (~180 μm) was obtained from Qingdao BCSM Co., Ltd. Water used in this work was purified by a Milli-Q water system (Millipore, USA).

2.2 GO synthesis

Graphite oxide was obtained with Hummers' method.[35,36] Briefly, graphite oxide was obtained by the oxidation of 3 g of graphite with 400 mL of H_2SO_4, and 18 g of $KMnO_4$. The mixture was stirred for three days to ensure the complete oxidation of the graphite. Then, H_2O_2 solution was added to stop the oxidation process, and the color of the mixture changed to bright yellow, indicating a high oxidation level of graphite. The formed graphite oxide was washed three times with 1.0 M aqueous HCl solution and repeatedly with deionized water until a pH of 4–5 was achieved. Then, the obtained graphite oxide dispersion was exposed to ultrasonication for 2 h, followed by centrifugation to remove unexfoliated graphite oxide. Finally, the sample was freeze-dried to obtain the GO solid.

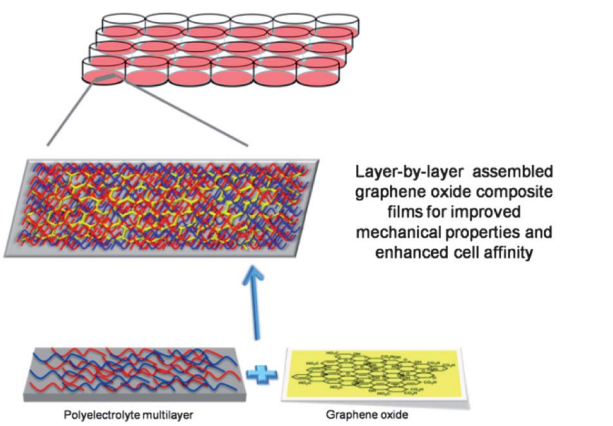

Scheme 1 Schematic representation of the construction of layer-by-layer assembled GO nanocomposite and its effects on NIH-3T3 cell behavior.

2.3 Multilayer film preparation

14 mm diameter glass coverslips used as substrates for the LbL assembly were cleaned in piranha solution (7 : 3 v/v H_2SO_4–H_2O_2) before use, followed by rinsing with water. Polyelectrolyte solutions were prepared by the dissolution of the polyelectrolyte powders at a concentration of 2 mg mL^{-1} in 0.2 M NaCl solution, and GO dispersion was prepared at a concentration of 0.1 mg mL^{-1} in water. For all the films, a precursor layer of PEI was deposited on the substrate. PSS, PAH and GO were then alternately assembled onto the substrate. There were 15–20 minutes for each deposited layer and three rinses in water. Five different types of film have been prepared, as follows: $(PAH/PSS)_{11}$ film, $(PAH/PSS)_5/PAH/GO/(PAH/PSS)_5$ film, $[(PAH/PSS)_2/PAH/GO/(PAH/PSS)_2]_2/PAH/PSS$ film, $(PAH/PSS/PAH/GO)_5/PAH/PSS$ film and $(PAH/GO)_{10}/PAH/PSS$ film. These all consist of 11 bilayers in total.

2.4 Film characterization

The growth and microstructure of the multilayer films were characterized by UV-vis spectroscopy (UV-1601, Shimadzu, Japan), QCM (Chenhua Co., Shanghai, China) and AFM (Digital Instruments, USA).

Nanomechanical tests were carried out using a Triboindenter from Hysitron Inc (USA), a load-controlled, displacement-sensing device.[37,38] The measurement was performed with a temperature of 20–25 °C and with a humidity of about 30%. A Berkovich diamond indenter was employed with a tip radius in the range of 100–200 nm. A trapezoidal loading pattern consisting of a 5 s loading segment, a 2 s hold period, and a 5 s unloading segment was used for all tests. The unloading segment of the P–h curve was utilized for the extraction of the mechanical properties, based on the method of Oliver and Pharr. The elastic modulus E_r and the sample hardness H were computed from three measured parameters: the peak load, P_{max}, the peak displacement, h_{max}, and the contact stiffness, $S = dP/dh$. S is determined by curve fitting the upper portion of the unloading curve and measuring its slope at P_{max}.

2.5 Cell culture

NIH-3T3, a mouse embryonic fibroblast cell line, cells were cultured in Dulbecco's modified Eagle's medium (DMEM) containing 4.5 g L^{-1} D-glucose and supplemented with fetal bovine serum (10%), penicillin (100 units mL^{-1}), and streptomycin (100 μg mL^{-1}) at 37 °C in a 5% CO_2 environment.[8]

2.6 Cell viability

For cell viability, the 3T3 cells were seeded on the five different types of films, namely, $(PAH/PSS)_{11}$ film, $(PAH/PSS)_5/PAH/GO/(PAH/PSS)_5$ film, $[(PAH/PSS)_2/PAH/GO/(PAH/PSS)_2]_2/PAH/PSS$ film, $(PAH/PSS/PAH/GO)_5/PAH/PSS$ film and $(PAH/GO)_{10}/PAH/PSS$ film, and on the coverslip as a control. MTT assays were carried out for all the above cells. The filtered 3-(4,5-dimethylthiazol-2-yl)-2,5-diphenyltetrazolium bromide (MTT, sigma, USA) solution was added to the cell cultures in turn at 2 h, 2 days and 7 days after seeding. The cell viability was measured at 570 nm using UV-vis spectroscopy.

2.7 Focal adhesion imaging and quantification

Cells were plated on the different films and were cultured at 37 °C in the presence of serum. The film coated slides were removed from the culture at 24 h after plating, then washed with PBS, and fixed in 3.7% paraformaldehyde for 4 min. The slides were washed with PBS and further treated with 0.1% Triton X-100 in PBS for 1 min and blocking solution (goat serum) for 30 min. To visualize focal adhesion, the cells were treated with anti-vinculin antibody (Sigma, USA) diluted 1 : 200 in blocking solution for 1 h, followed by incubation with goat anti-mouse DyLight® 594 conjugated antibody (Thermo Fisher Scientific, USA) at 1 : 400 dilution in blocking buffer for 1 h. For double labeling, FITC-phalloidin was incubated simultaneously with the second antibody. The slides were washed three times with PBS between each antibody treatment.[8] They were viewed through an Olympus confocal microscope system FV 1000 (Olympus, Japan). The focal adhesion size and spatial distribution were analyzed using ImageJ software (NIH, USA).

2.8 Statistical analysis

All experiments were repeated at least three times. Error bars represent standard errors, and statistical analysis was performed using SPSS 13.0 to evaluate the statistical differences (<0.05) among all the samples or between samples and controls.

3 Results and discussion

3.1 Nanocomposite film buildup

GO was prepared by chemical oxidation from natural graphite. Briefly, graphite was first oxidized to form graphite oxide and then exfoliated to GO. Fig. 1 shows an AFM image of GO nanosheets on silicon wafers. Analysis of the AFM images shows that the GO nanosheets had heights of ~1.0 nm, which is the characteristic thickness of GO nanosheets.[31,39]

The buildup of the PAH/GO film was monitored by UV-vis absorption spectra and measured after each cycle of the deposition. The typical LbL deposition process was performed by coating quartz slides with PAH, PSS or GO alternately. The UV-vis absorption spectra of the PAH/GO film within the first 10 cycles are shown in Fig. 2a. They all exhibit two characteristic features that can be used as a means of identification: a maximum at 231 nm, corresponding to the π–π* transitions of aromatic C–C bonds, and a shoulder at ~300 nm, which can be attributed to the n–π* transitions of C=O bonds.[39] It is of note that a progressive increase in absorbance at these wavelengths was visible as the number of bilayers increased, indicating a uniform LbL assembly process.

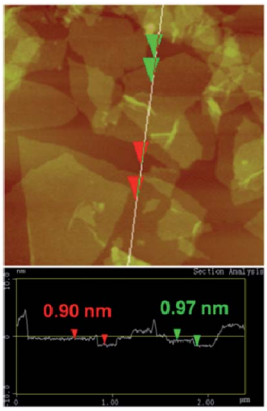

Fig. 1 AFM image (2.5 × 2.5 μm^2) of GO nanosheets deposited onto a silicon wafer from an aqueous dispersion. The line profile for the sheet is marked by the white line in the image, indicating the thickness of the GO nanosheets.

Additionally, the buildup of the films was followed by QCM measurements at 8 MHz resonance frequency of the quartz crystal. Fig. 2b represents the evolution of the frequency shifts during the film buildup process. As expected, the frequency decreased with each polyelectrolyte or GO injection, indicating that mass is added during each deposition step. A higher decrease in frequency was recorded for the PAH/GO film, while smaller changes were observed for the PAH/PSS films, suggesting an increased adsorbed mass for the former. Accordingly, the PAH/GO film could be expected to be thicker and stiffer than the PAH/PSS film. This may be confirmed by AFM measurements.

3.2 Characterization of surface roughness and mechanical properties of the film

AFM was used to analyze the surface topographies, roughness and thickness of the PAH/PSS and PAH/GO films. Fig. 3 shows the tapping-mode AFM images of the $(PAH/PSS)_{11}$ film (Fig. 3a) and the $(PAH/GO)_{10}/PAH/PSS$ film (Fig. 3b) deposited on glass coverslips. One can notice that AFM images reveal the presence of nanometer sized GO nanosheets on the nanocomposite film surface. The difference in the components of the two types of films is also shown in the phase images (Fig. 3c and d). The thickness and surface roughness of these two types of film are summarized in Table 1. The thickness for the $(PAH/PSS)_{11}$ film is 9.63 nm with a roughness of 6.34 nm. The $(PAH/GO)_{10}/PAH/PSS$ film, with a thickness of 29.9 nm, was much thicker than the $(PAH/PSS)_{11}$ film, which is consistent with the QCM data. However, the film top surface of the former (Rms = 4.91 nm) was smoother than that of the latter. Thus, the PEM films could be thicker and smoother with the incorporation of GO in the polymeric matrix.

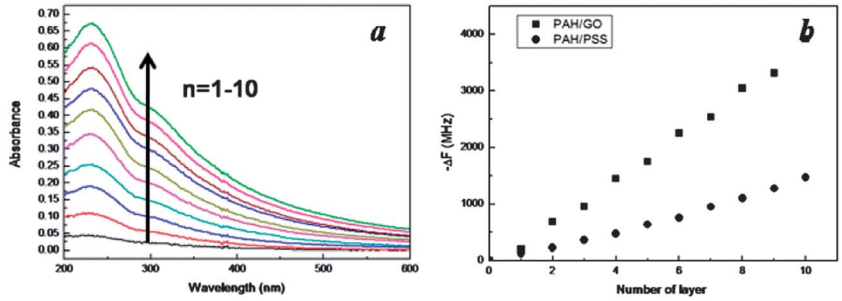

Fig. 2 (a) UV absorption spectra of $(PAH/GO)_n$ film. The number of bilayers is 1–10 from the bottom to the top. (b) Film growth followed by *in situ* QCM. Differences in the frequency shifts measured at the end of each polycation and polyanion deposition for $(PAH/GO)_n$ and $(PAH/PSS)_n$, n = 1–10.

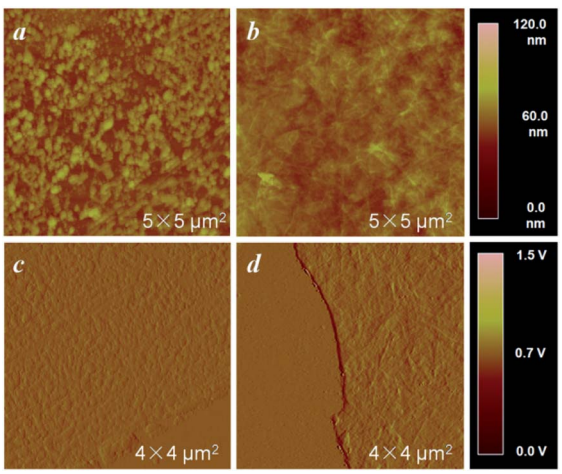

Fig. 3 AFM images showing surface morphology of (a) $(PAH/PSS)_{11}$ and (b) $(PAH/GO)_{10}$/PAH/PSS multilayer films. (c) and (d) are the phase images of the $(PAH/PSS)_{11}$ and $(PAH/GO)_{10}$/PAH/PSS films, respectively.

Table 1 The thickness and roughness of the $(PAH/PSS)_{11}$ film and $(PAH/GO)_{10}$/PAH/PSS film as measured by AFM software

Multilayer film	Film thickness (nm)	Film roughness (Rms) (nm)
$(PAH/PSS)_{11}$	9.63	6.34
$(PAH/GO)_{10}$/PAH/PSS	29.9	4.91

Next, the mechanical properties of the films were measured by means of a Triboindenter *in situ* nanomechanical test system. Nanoindentation is a useful tool that allows the direct measurement of the mechanical properties of thin films. By indentation of a material to a desired force (or depth) followed by retraction of the tip, a force–displacement (P–h) curve, characteristic of the material being tested, is obtained.[40] The elastic modulus (E_r) and hardness (H) can be obtained by analysis of this curve. In this work, five types of film, that is, $(PAH/PSS)_{330}$, $[(PAH/PSS)_5/PAH/GO/(PAH/PSS)_5]_{30}$, $[(PAH/PSS)_2/PAH/GO/(PAH/PSS)_2]_{66}$, $(PAH/PSS/PAH/GO/PAH/PSS)_{110}$, and $[(PAH/GO)_{10}/PAH/PSS]_{30}$ were designed to tune the mechanical properties of the composite films by changing the number of layers of GO. All the films were constructed up to 330 bilayers in all to ignore the influence of the mechanical properties of the underlying substrate. For the five types of films, P–h curves were obtained (Fig. 4a) and the average values of E_r and H derived by Oliver and Pharr's method varied with the proportion of GO as displayed in Fig. 4b and c, respectively. The results show a significant enhancement of E_r and H of the LbL composite films with the increase in GO content. The E_r value was 3.37 GPa for the $(PAH/PSS)_{330}$ film and it increased to 18.8 GPa for the $[(PAH/GO)_{10}/PAH/PSS]_{30}$ film, an enhancement of over 5-fold. Notably, a 181% improvement of E_r was also observed when one layer of GO was incorporated between five PAA/PAH bilayers, that is in the $[(PAH/PSS)_5/PAH/GO/(PAH/PSS)_5]_{30}$ film. Additionally, the films became stiffer when the GO content continued to be increased and nearly reached a plateau when one layer of GO was between one PAH/PSS bilayer, that is in the $(PAH/PSS/PAH/GO/PAH/PSS)_{110}$ film. Additionally, an increasing tendency for hardness was observed obviously for these films. The H value of the $[(PAH/GO)_{10}/PAH/PSS]_{30}$ film appeared to be approximately ten times higher than that of the $(PAH/PSS)_{330}$ film. Hence, the mechanical properties of the composite films could be modified significantly by the incorporation of GO into the polyelectrolyte matrix. Herein, the enhanced mechanical properties may be attributed to the ability of LbL technique to immobilize the high strength material inside of the polymeric matrix, which allows for more effective and higher loading without phase segregation than in many other composites.[12]

3.3 Cell response to the film

Given the potential use of the films in the biomedical field, NIH-3T3 cell viability cultured on each type of film were evaluated using live/dead staining with calcein-AM (to stain live cells with a green color) and ethidium homodimer (to stain dead cells with a red color). Fluorescence microscopy revealed that most of the cells plated were alive on the films including the $(PAH/PSS)_{11}$ film, the $(PAH/PSS)_5/PAH/GO/(PAH/PSS)_5$ film, the $[(PAH/PSS)_2/PAH/GO/(PAH/PSS)_2]_2/PAH/PSS$ film, the $(PAH/PSS/PAH/GO)_5/PAH/PSS$ film and the $(PAH/GO)_{10}/PAH/PSS$ film. For example, Fig. 5a and b show the fluorescent images of cells on the $(PAH/PSS)_{11}$ film and the $(PAH/GO)_{10}/PAH/PSS$ film after

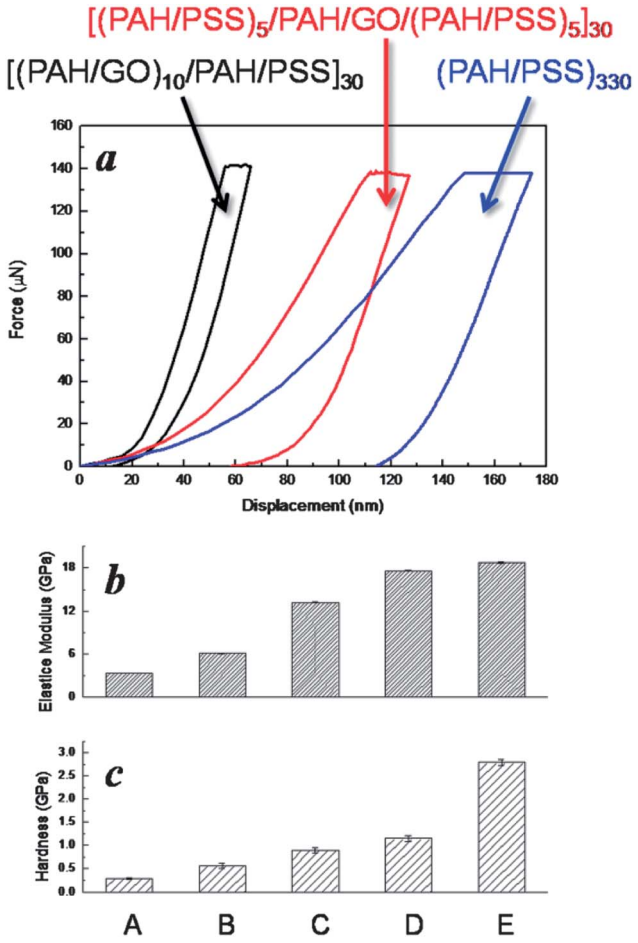

Fig. 4 (a) Force–displacement curves of $(PAH/PSS)_{330}$, $[(PAH/PSS)_5/PAH/GO/(PAH/PSS)_5]_{30}$ and $[(PAH/GO)_{10}/PAH/PSS]_{30}$ films. Values of elastic modulus (b) and hardness (c) for LbL multilayer films: (A) $(PAH/PSS)_{330}$; (B) $[(PAH/PSS)_5/PAH/GO/(PAH/PSS)_5]_{30}$; (C) $[(PAH/PSS)_2/PAH/GO/(PAH/PSS)_2]_{66}$; (D) $(PAH/PSS/PAH/GO/PAH/PSS)_{110}$; (E) $[(PAH/GO)_{10}/PAH/PSS]_{30}$.

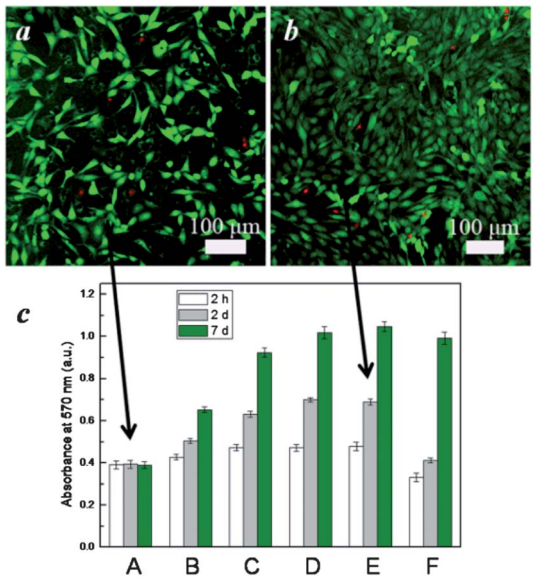

Fig. 5 Fluorescence images of the cells obtained on (a) $(PAH/PSS)_{11}$ and (b) $(PAH/GO)_{10}/PAH/PSS$ films by live/dead staining of NIH-3T3 cells after incubation for 48 h. Live cells are stained fluorescent green, and dead cells appear red. (c) Cell viabilities (MTT test) measured at 2 h, 2 days and 7 days on films including (A) $(PAH/PSS)_{11}$; (B) $(PAH/PSS)_5/PAH/GO/(PAH/PSS)_5$; (C) $[(PAH/PSS)_2/PAH/GO/(PAH/PSS)_2]_2/PAH/PSS$; (D) $(PAH/PSS/PAH/GO)_5/PAH/PSS$; (E) $(PAH/GO)_{10}/PAH/PSS$; (F) glass coverslips as a control.

48 h seeding. Furthermore, cell viabilities (Fig. 5c) were determined on five types of film using the MTT colorimetric assay at different time intervals (0, 2 and 7 days). The proliferation rate was estimated by the ratio of absorbance of d7 over that of d0. For the $(PAH/PSS)_{11}$ films, the cells nearly did not proliferate. On the contrary, cells grown on the $[(PAH/PSS)_2/PAH/GO/(PAH/PSS)_2]_2/PAH/PSS$ films had a proliferation rate of 196%, and the cells cultured on the $(PAH/GO)_{10}/PAH/PSS$ films proliferated 219%. The results of the cell viability and proliferation assay indicated that all of the investigated films could be considered cell-friendly, and especially that the GO composite films were more favorable to cell proliferation compared with the native PEM films.

Cell adhesion is a fundamental process directly involved in cell growth, cell migration, and cell differentiation. It is involved in embryogenesis, the maintenance of tissue integrity, wound healing, immune response, cancer metastasis, and biomaterial tissue integration.[41] Moreover, previous reports have shown that cells could sense their microenvironment and respond by adjusting the organization of their cytoskeleton and the formation of focal adhesion points which specifically bind the cell to the surface.[42,43] Herein, the NIH-3T3 cell adhesion behavior was investigated on the five types of film studied. The cells were first fixed and immunofluorescently stained for vinculin and F-actin to study whether focal adhesion and actin stress fiber organization were affected by the films. The organization of actin was examined by fluorescence microscopy after 24 h in culture using FITC-labeled phalloidin which binds specifically to filamentous actin. The cells were found attached efficiently to each of the films. In fact, there were no significant differences in the cytoskeleton structure of the cells on the five types of films (Fig. 6). The cells contain a prominent system of filament bundles or stress fibers and no prominent staining is revealed in the cell periphery. Simultaneously, the cells were stained with antivinculin antibody and a secondary antibody labeled with DyLight 549 to detect vinculin at focal adhesions. The image (Fig. 6) also revealed that antibody to vinculin intensely stained the ends of the stress fibers in the cells cultured on all the films. It is well established that vinculin plays a pivotal role in cell adhesion and migration by providing the link between the actin cytoskeleton and the transmembrane receptors, integrin and cadherin.[41,43] Here, the vinculin plaques at the stress fiber ends were triangular and sharply delineated. But for the cells on the glass covers, they had a peripheral actin distribution with no stress fiber formation and diffuse vinculin localization. In contrast, the cells cultured on all the film-coating substrates showed well-organized F-actin stress fibers as well as numerous, large and mature focal adhesions implying that the cytoskeleton organization was enhanced on these films.

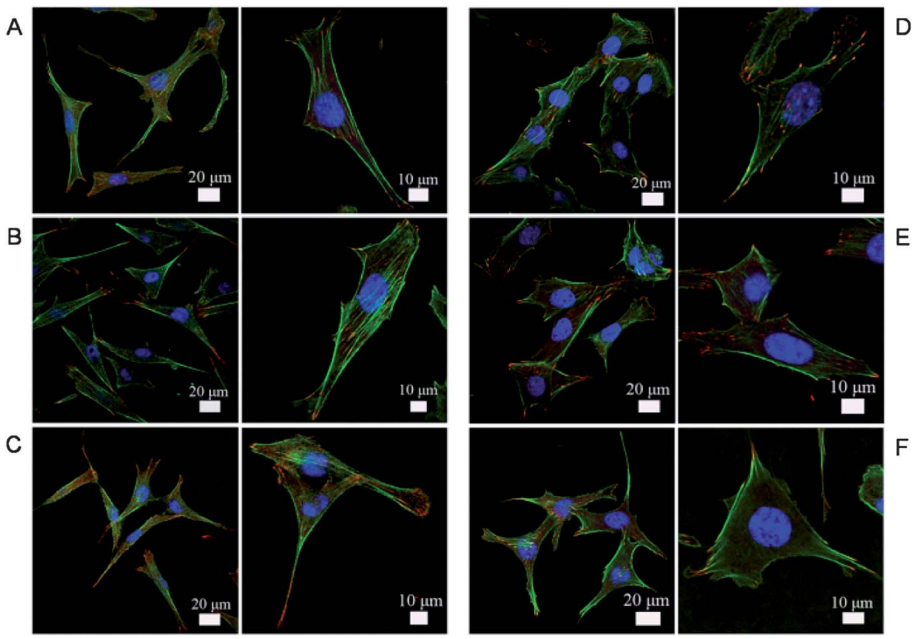

Fig. 6 Confocal laser scanning microscopy images of cell adhesion on the films including (A) $(PAH/PSS)_{11}$; (B) $(PAH/PSS)_5/PAH/GO/(PAH/PSS)_5$; (C) $[(PAH/PSS)_2/PAH/GO/(PAH/PSS)_2]_2/PAH/PSS$; (D) $(PAH/PSS/PAH/GO)_5/PAH/PSS$; (E) $(PAH/GO)_{10}/PAH/PSS$; (F) glass coverslips. NIH-3T3 cells were incubated on each type of film for 24 h, and then actin and vinculin were stained with phalloidin-FITC (green) and a monoclonal antivinculin antibody (red), respectively. The scale bars are 20 μm for the left image of each series, and 10 μm for the enlarged images.

Next, quantitative area analysis of cell spreading and number of focal adhesions on the five types of films were conducted using ImageJ software (Fig. 7). The cell spreading areas were observed to increase steadily in the range of 1806–2344 μm^2 per cell with the increase of GO content. Higher values of 2288 and 2344 μm^2 per cell could be reached for the $(PAH/PSS/PAH/GO)_5/PAH/PSS$ film and the $(PAH/GO)_{10}/PAH/PSS$ film, respectively. Quantitative analysis of focal adhesions showed that the cells adherent to the $(PAH/PSS/PAH/GO)_5/PAH/PSS$ films had 1.6 times more FAs than those to the $(PAH/PSS)_{11}$ films. The FAs formed in cells on the $(PAH/GO)_{10}/PAH/PSS$ film were approximately equal to those of the $(PAH/PSS/PAH/GO)_5/PAH/PSS$ film.

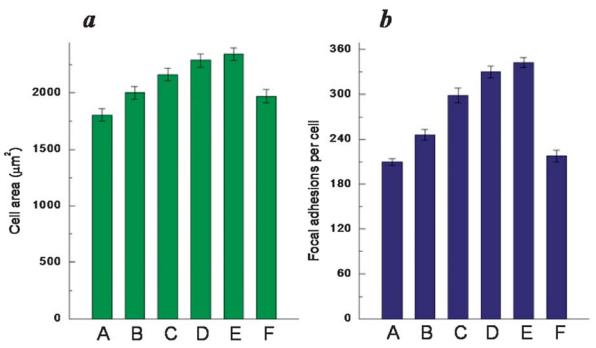

Fig. 7 Quantitative analysis of (a) cell spreading area and (b) average focal adhesion number per cell on the films including (A) $(PAH/PSS)_{11}$; (B) $(PAH/PSS)_5/PAH/GO/(PAH/PSS)_5$; (C) $[(PAH/PSS)_2/PAH/GO/(PAH/PSS)_2]_2/PAH/PSS$; (D) $(PAH/PSS/PAH/GO)_5/PAH/PSS$; (E) $(PAH/GO)_{10}/PAH/PSS$; (F) glass coverslip.

Taken together, compared with the PEM films, the cells showed larger cell spreading areas and more focal adhesion points on the nanocomposite films. It may be concluded that the NIH-3T3 cells could obtain higher affinity for the GO composite films than for the native PEM films. The same final layers, PAH/PSS, were used so that the effect of chemical composition on the cellular processes was ignored. The mechanical properties of the films may play roles in the cell response to the surfaces,[44–46] however, the thickness and topography might not be ruled out. For a better understanding of the effects of the physicochemical properties on the cell behavior, it would be ideal to test the films similar in some properties, and different only in one certain property. This will be performed in detail in the coming work.

4 Conclusions

In this work, the GO nanocomposites were constructed *via* the LbL assembly technique. GO nanosheets were incorporated into the polymeric matrix to tune and improve the mechanical properties of the PEM films. It was demonstrated that both the elastic modulus and hardness of the nanocomposites could increase significantly with the incorporation of GO. Additionally, the mechanical properties of the film can be tailored by varying number of layers of GO in the multilayer. Furthermore, the effects of the nanocomposites on NIH-3T3 cell adhesion and proliferation were investigated. The cell response results showed that the NIH-3T3 cell could adhere well to and develop

on the nanocomposite films. Obviously, compared with the native PEM film, the cells proliferated faster, spread more, and developed more numerous and better organized adhesion points on the GO nanocomposite films. Although the relationship between cell adhesion and the nanocomposite film is far from being understood, the results confirmed that the mechanical properties of PEM films could be tuned and controlled for improved cell–substrate interactions by simply choosing inorganic nanomaterials. It is of particular interest that the LbL method offers the possibility of combining different kinds of components in a multi-functional platform. There is no doubt that these systems are encouraging for the preparation of novel, high strength materials.

Acknowledgements

This work was financially supported by the National Nature Science Foundation of China (no. 21003084, 21375075), Shandong Province Promotive Research Foundation for Excellent Young and Middle-Aged Scientists (no. BS2010CL023), Student Research Training Program of Qufu Normal University (no. 201210446022, 2013A046), and the Taishan Scholar Foundation of Shandong Province, China.

Notes and references

1 G. Decher, *Science*, 1997, **277**, 1232.
2 K. Ariga, J. P. Hill and Q. Ji, *Phys. Chem. Chem. Phys.*, 2007, **9**, 2319.
3 K. Ariga, Q. Ji, J. P. Hill1, Y. Bando and M. Aono, *NPG Asia Mater.*, 2012, **4**, e17, DOI: 10.1038/am.2012.30.
4 K. Ariga, Q. M. Ji, T. Mori, M. Naito, Y. Yamauchi, H. Abec and J. P. Hill, *Chem. Soc. Rev.*, 2013, **42**, 6322.
5 Y. Jia, Y. Cui, J. B. Fei, M. C. Du, L. R. Dai, J. B. Li and Y. Yang, *Adv. Funct. Mater.*, 2012, **22**, 1446.
6 W. Qi, M. Sun and Z. H. Jing, *Supramol. Chem.*, 2012, **24**, 350.
7 J. Zhao, Y. Cui, A. H. Wang, J. B. Fei, Y. Yang and J. B. Li, *Langmuir*, 2011, **27**, 1499.
8 S.-R. Ryoo, Y.-K. Kim, M.-H. Kim and D.-H. Min, *ACS Nano*, 2010, **11**, 6587–6598.
9 L. Chen, H. Thérien-Aubin, M. C. Y. Wong, E. M. V. Hoekcde and C. K. Ober, *J. Mater. Chem. B*, 2013, **1**, 5651.
10 C. Y. Jiang and V. V. Tsukruk, *Adv. Mater.*, 2006, **18**, 829.
11 T. Boudou, T. Crouzier, C. Nicolas, K. F. Ren and C. Picart, *Macromol. Biosci.*, 2011, **11**, 77.
12 P. Podsiadlo, Z. Y. Tang, B. S. Shim and N. A. Kotov, *Nano Lett.*, 2007, **7**, 1224.
13 J. Zhu, H. Zhang and N. A. Kotov, *ACS Nano*, 2013, **7**, 4818.
14 J. A. Phelps, S. Morisse, M. Hindie, M.-C. Degat, E. Pauthe and P. R. Van Tassel, *Langmuir*, 2011, **27**, 1123.
15 A. Schneider, G. Francius, R. Obeid, P. Schwinté, J. Hemmerlé, B. Frisch, P. Schaaf, J.-C. Voegel, B. Senger and C. Picart, *Langmuir*, 2006, **22**, 1193.
16 J. Blacklock, A. Vetter, A. Lankenau, D. Oupický and H. Möhwald, *Biomaterials*, 2010, **31**, 7167.
17 K. Ariga, T. Mori and J. P. Hill, *Adv. Mater.*, 2012, **24**, 158–176.
18 K. Ariga, A. Vinu, Y. Yamauchi, Q. Ji and J. P. Hill, *Bull. Chem. Soc. Jpn.*, 2012, **85**, 1–32.
19 L. Feng, X. Yang, X. Shi, X. Tan, R. Peng, J. Wang and Z. Liu, *Small*, 2013, **9**, 1989.
20 K. Yang, H. Gong, X. Shi, J. Wan, Y. Zhang and Z. Liu, *Biomaterials*, 2013, **34**, 2787.
21 J. H. Jung, D. S. Cheon, F. Liu, K. B. Lee and T. S. Seo, *Angew. Chem., Int. Ed.*, 2010, **49**, 5708.
22 K. S. Novoselov, A. K. Geim, S. V. Morozov, D. Jiang, Y. Zhang, S. V. Dubonos, I. V. Grigorieva and A. A. Firsov, *Science*, 2004, **306**, 666.
23 Y. P. Zhang and C. X. Pan, *Diamond Relat. Mater.*, 2012, **24**, 1.
24 C. G. Lee, X. D. Wei, J. W. Kysar and J. Hone, *Science*, 2008, **321**, 385.
25 Y. Wang, Z. H. Li, J. Wang, J. H. Li and Y. H. Lin, *Trends Biotechnol.*, 2011, **29**, 205.
26 C. Chung, Y.-K. Kim, D. Shin, S.-R. Ryoo, B. H. Hong and D.-H. Min, *Acc. Chem. Res.*, 2013, **46**, 2211.
27 J. Kim, L. J. Cote and J. X. Huang, *Acc. Chem. Res.*, 2012, **45**, 1356.
28 J. Hong, N. J. Shah, A. C. Drake, P. C. DeMuth, J. B. Lee, J. Chen and P. T. Hammond, *ACS Nano*, 2012, **6**(1), 81.
29 Q. Ji, I. Honma, S.-M. Paek, M. Akada, J. P. Hill, A. Vinu and K. Ariga, *Angew. Chem., Int. Ed.*, 2010, **49**, 9737.
30 X. Zhao, Q. H. Zhang, Y. P. Hao, Y. Z. Li, Y. Fang and D. J. Chen, *Macromolecules*, 2010, **43**, 9411.
31 K. S. Choi, F. Liu, J. S. Choi and T. S. Seo, *Langmuir*, 2010, **26**, 12902.
32 D. Y. Cai and M. Song, *J. Mater. Chem.*, 2010, **20**, 7906.
33 D. W. Lee, T.-K. Hong, D. Kang, J. Lee, M. Heo, J. Y. Kim, B.-S. Kim and H. S. Shin, *J. Mater. Chem.*, 2011, **21**, 3438.
34 H. H. Oh, Y.-G. Ko, H. Lu, N. Kawazoe and G. Chen, *Adv. Mater.*, 2012, **24**, 4311.
35 W. S. Hummers and R. E. Offeman, *J. Am. Chem. Soc.*, 1958, **80**, 1339.
36 H. N. Lim, N. M. Huang, S. S. Lim, I. Harrison and C. H. Chia, *Int. J. Nanomed.*, 2011, **6**, 1817.
37 A. J. Nolte, M. F. Rubner and R. E. Cohen, *Macromolecules*, 2005, **38**, 5367.
38 T. Y. Tsui, W. C. Oliver and G. M. Pharr, *J. Mater. Res.*, 1996, **11**, 752.
39 J. I. Paredes, S. Villar-Rodil, A. Martínez-Alonso and J. M. D. Tascón, *Langmuir*, 2008, **24**, 10560.
40 P. V. Pavoor, A. Bellare, A. Strom, D. H. Yang and R. E. Cohen, *Macromolecules*, 2004, **37**, 4865–4871.
41 M. Schliwa, T. Nakamura, K. R. Porter and U. Euteneuer, *J. Cell Biol.*, 1984, **99**, 1045.
42 L. L. Han, Z. W. Mao, J. D. Wu, Y. Y. Zhang and C. Y. Gao, *J. R. Soc., Interface*, 2012, **9**, 3455.
43 M. Kato and M. Mrksich, *Biochemistry*, 2004, **43**, 2699.
44 D. E. Discher, P. Janmey and Y. L. Wang, *Science*, 2005, **310**, 1139–1143.
45 J. K. Van Tam, K. Uto, M. Ebara, S. Pagliari, G. Forte and T. Aoyagi, *Sci. Technol. Adv. Mater.*, 2012, **13**, 064205.
46 S. Even-Ram, V. Artym and K. M. Yamada, *Cell*, 2006, **126**, 645.